

9.85 Lightning Initiation Forecasting: An Operational Dual-Polarimetric Radar Technique

Crystal J. Woodard*¹, Lawrence D. Carey¹, Walter A. Petersen²,
William P. Roeder³

¹ University of Alabama in Huntsville ² NASA MSFC, Huntsville, AL
³ 45th Weather Squadron, Patrick AFB, FL

1. INTRODUCTION

Lightning is one of Earth's natural dangers, destructive not only to life but also physical property. According to the National Weather Service, there are on average 58 lightning fatalities each year, with over 300 related injuries (National Weather Service 2010). Most of these fatalities and injuries are incurred during outdoor activities. Various activities emphasize a need for different initiation forecasting skill. For example, the ability to accurately forecast total lightning is critical to space vehicle launch operations. The 45th Weather Squadron (45 WS) issues lightning watches and warnings for Cape Canaveral Air Force Station, NASA Kennedy Space Center, Patrick Air Force Base, and other locations (McNamara et al., 2010). These lightning watches and warnings provide safety for over 25,000 personnel and facilities worth over twenty billion dollars. Forecasting lightning is also part of forecasting Lightning Launch Commit Criteria to protect in-flight space launch vehicles from natural and rocket-triggered lightning that could cause billions of dollars of damage and possible loss of life (McNamara et al., 2010). Lightning forecasting that provides longer lead times could provide officials of large outdoor venues with more time to respond to possible threatening weather events.

Many researchers have developed and tested different methods and tools of first flash forecasting, however few have done so using dual-polarimetric radar variables and products on an operational basis. The purpose of this study is to improve algorithms for the short-term prediction of lightning initiation through development and testing of operational techniques that rely on parameters observed and diagnosed using C-band dual-polarimetric radar. Dual-polarimetric observations provide

Corresponding author address: Crystal Woodard, ESSC/NSSTC, 320 Sparkman Dr., Huntsville, AL 35805; email: woodarcj@nsstc.uah.edu

enhanced information on hydrometeor types, effective shape and amounts. According to most studies, significant electrification and first flash occurrence in thunderstorms rely on the presence of specific hydrometeors (such as graupel and hail) (Workman and Reynolds 1949; Reynolds et al. 1957; Church 1966; Takahashi 1978; Dye et al. 1986, 1988, 1992; Goodman et al. 1988; Keith and Saunders 1990; Saunders et al. 1991; Rutledge and Petersen 1994; Carey and Rutledge 1996, 2000). As such, we explore the hypothesis that the use of dual-polarimetric variables should significantly improve current radar reflectivity based first flash forecasting. For example, the 45th Weather Squadron has used reflectivity ≥ 35 dBZ reaching -10°C with a depth of ≥ 3000 Ft above that level for $\geq 10 - 20$ min to forecast the first lightning flash, including lightning aloft (Roeder and Pinder 1998).

2. METHODOLOGY AND TOOLS

Using the University of Alabama in Huntsville-Northern Alabama area C-band dual-polarimetric radar, ARMOR (Advanced Radar for Meteorological and Operational Research), data is collected on ordinary convective storms (Petersen et al. 2007). Ordinary convective cells are generally isolated, pulse type storms, weak in comparison to supercellular and multicellular storm structures. An optimized PPI (plan position indicator) sector volume scan with excellent vertical coverage of the storm was used to collect data on cells from initial formation to first flash or dissipation. The scan strategy employed consists of a sector volume scan repeated every two to five minutes for temporal data quality. To further ensure data quality at significant observation levels for cloud electrification and lightning production (e.g., 0 to -20°C), a maximum range of evaluation is also established based upon the scan strategy and vertical temperature profile. The vertical temperature profile soundings used are provided by the Redstone Arsenal in Huntsville or derived

using a linear average of the Birmingham and Nashville soundings. To observe individual cellular microphysical processes, the cells are evaluated for spatial distinction from other convective systems and radar coverage. This means that each cell is observable within the radar sector volume scans from initial formation to first flash and must be distinguishable and relatively independent from convective systems, such as a squall line, where cells typically closely interact. The first lightning flash (either inner-cloud lightning or cloud-to-ground lightning) is determined using the NAL LMA (Northern Alabama Lightning Mapping Array), a network of 10 time-of-arrival VHF total lightning sensors, as mapped in Fig. 1 (Goodman et al. 2005). NAL LMA reports on the time and location of the source of VHF signals associated with lightning. To ensure the accuracy of the source data, the first flash is determined by the location of the first VHF source as reported by a source-to-flash algorithm (McCaul et al. 2005). For data quality purposes, ARMOR horizontal radar reflectivity (Z_h) and differential reflectivity (Z_{DR}) are routinely calibrated using dual-polarimetric techniques (Bringi and Chandrasekar 2001; Ryzhkov et al. 2005). The ARMOR Z_h and Z_{DR} are furthermore corrected for precipitation attenuation and differential attenuation, respectively (Bringi et al. 2001).

The radar data are further processed by a C-band polarimetric radar modified NCAR fuzzy-logic based particle identification (PID) algorithm using Z_h , Z_{DR} , correlation coefficient (ρ_{hv}), specific phase shift (K_{DP}) and the temperature profile as inputs. The PID algorithm estimates the hydrometeor types associated with the values of the radar variables (Deierling et al. 2008, Vivekanandan et al. 1999). Radar reflectivity provides an estimate of relative drop size concentration. High values of Z_h , such as 45 dBZ, are indicative of a concentration of mm-sized particles, such as graupel. Z_{DR} is the estimated reflectivity weighted measure of particle oblateness. Values of Z_{DR} near zero ($Z_{DR} < 0.5$ dB) indicate apparent spherical hydrometeors, such as tumbling hail stones or small rain drops. Larger values, greater than 0.5 dB, are associated with oblate spheres such as large raindrops. This parameter, combined with reflectivity, is also useful in hydrometeor identification as discussed later. K_{DP} is the difference in horizontal and vertical phase shift of the radar signal at a specific radar volume. It assists in the estimation of the physical phase of the hydrometeors in a radar volume as it is

dependent on the radar signal's propagation speeds. ρ_{hv} is the correlation, or similarity, between the horizontal and vertical pulse signals received by the radar. A well correlated radar volume will have a value near 1, such as a volume of uniform raindrops. Non-hydrometeors, such as insects, produce values less than 0.8. Due to the sensitivity and relative error associated with this process, the hydrometeor types are evaluated based on condensed bulk hydrometeor classification categories to ensure accurate classification.

After the data are fully processed, an area of interest, or "Larsen area" (Larsen and Stansbury 1974), is visually assessed for each cell that meets the previously stated criteria. The Larsen area is defined by a Z_h reflectivity threshold at a significant thermal level related to charging mechanisms. This study defines the Larsen area as an area with a diameter encompassing the 30 dBZ reflectivity echo at -10°C as demonstrated in Fig. 2. The thermal level is based on the NIC (non-inductive charging) method in which charge separation occurs by chance collision of large ice particles with smaller ice crystals in the presence of supercooled liquid (Reynolds et al. 1957). The -10°C level is approximately the lower level of the main negative charge layer of the tripole charge structure created by storm-scale charge separation (MacGorman and Rust 1998). Reflectivity values greater than 30 dBZ imply the likely presence of larger precipitation sizes, such as mm-sized graupel and small hail, in concentrations required for significant electrification. Visual tools such as SOLOII, an NCAR radar sweep file viewer, and ANGEL (Analysis of NEXRAD, GPS, EDOT, and LMA), UF (universal format) radar and LMA lightning viewer, are used to evaluate cells.

Once a cell of interest is identified and defined, the test algorithms listed in Table 1 are applied to the data. Polarimetric radar parameters within the area of interest from levels above and below the target height that approximately meet the test criteria are extracted from the data to a text file. These values are then evaluated and interpolated.

The Z_h and temperature thresholds provide a crude means of hydrometeor identification and a means of comparison to previous studies. Reflectivity thresholds at a given temperature level have been previously studied and employed as a forecasting technique for non-polarized Doppler radars (Buechler and Goodman 1990, Dye et al. 1989, Gremillion and Orville 1999, Roeder and Pinder 1998, Vincent

et al 2003, Wolf 2007, Yang and King 2010). For example, reflectivity values above 35 dBZ associated with temperatures below freezing are consistent with the presence of mm-sized hydrometeors significant to electrification (i.e., graupel and hail). The various reflectivity thresholds are sensitivity tests consistent with previous studies conducted with 40 dBZ at -10°C as a benchmark. The benchmark is the leading “best method” of reflectivity based first flash forecasting in previous studies (Dye et al. 1989; Buechler and Goodman 1990; Gremillion and Orville 1999; Vincent et al. 2003; Wolf 2007, Yang and King 2010). “First instance” in this study is defined as the first occurrence of a single value (PID or dBZ) at a defined temperature threshold, as seen in Fig. 3. This can be a value linearly interpolated between two elevation scans for greater accuracy (as employed for Z_h). The secondary reflectivity level is a method of false alarm reduction by ensuring vertical development of the updraft as related to charge separation and NIC mechanism (Lhermitte and Krehviel 1979; Dye et al. 1989; Petersen et al. 1996). The 45 WS has used a depth of a reflectivity threshold above -10°C as part of their lightning forecasting since the early 1990s, along with duration and area (Roeder and Pinder 1998). 8 km is approximately in accordance to previous research which determined thunderstorm cloud top heights to peak over 7-9 km (Lhermitte and Krehviel 1979; Dye et al. 1986, 1989; Williams 1989; Petersen et al. 1996; Gremillion and Orville 1999; Carey and Rutledge 2000; Vincent et al. 2003).

The method of Z_{DR} column detection of oblate liquid hydrometeors is also a well studied method of hydrometeor identification associated with thunderstorm charging (Jameson et al. 1996; Bringi et al. 1997; Lund et al. 2009). Z_{DR} is a measure of reflectivity-weighted particle oblateness and is calculated as follows: $Z_{DR} = 10 \cdot \text{LOG}_{10}(z_h/z_v)$. Z_{DR} column is the association of high radar reflectivity values ($Z_h > 35$ dBZ) and enhanced values of Z_{DR} ($Z_{DR} > 0.5$ dB) representative of lofted raindrops above the freezing level, as can be examined in Fig. 4. A Z_{DR} column in warm cloud base storms that extends through the altitude of the freezing level is an indication that super-cooled raindrops exist that may later freeze into hail if the convective cell persists in time. These Z_{DR} column signatures could provide early warning of large precipitation ice and lightning.

PID is a modified NCAR fuzzy-logic based particle identification (PID) algorithm for C-band

polarimetric radar (Deierling et al. 2008, Vivekanandan et al. 1999). PID was chosen as a test variable for its ability to represent the wide suite of variables (previously discussed) that a dual-polarimetric radar is capable of producing and assisting the operator in real-time hydrometeor identification. These variables have been studied extensively and a trend of values for each dual-polarimetric parameter can be associated with particular hydrometeor types due to their innate characteristics (Lim et al. 2005, Vivekanandan et al. 1999). PID categories are based on bulk hydrometeor identification, meaning that each value is representative of the dominate hydrometeor signal in a volume of the storm which contains various hydrometeor sizes and types. This modified algorithm has 17 identification categories as listed in Table 2. For this reason categories are grouped together into lightning-relevant categories, e.g. graupel. Graupel and large ice particles are one of the key factors in cloud electrification.

3. RESULTS AND CONCLUSIONS

The data collected are obtained from eight case dates, from 2008 and 2010, producing a data set of 50 cells, 31 thunderstorm and 19 non-thunderstorm cells. These storms conform to the previously stated criteria, with the exception of two cells observed at a lower Larsen area requirement of 25 dBZ at -10°C to provide a more robust data set. The lower Larsen area requirement supports the assumption that cellular development that does not meet the higher Larsen area threshold does not generally produce lightning. The results of the test algorithms on these 50 cells can be seen in Tables 3 - 5.

The lead time is an average of lead times for all correctly forecasted events. POD, or probability of detection, is the ratio of correctly forecasted events to the total number of observed events (Jolliffe and Stephenson 2003). A perfect score of 1 indicates the accurate forecasting of positively occurring events. False alarm rate, FAR, is the ratio of falsely forecasted events to the number of forecasted events. A FAR value of 0 indicates the accuracy of the forecasting algorithm to indicate the occurrence or non-occurrence of an event. A score of 1 is not a negative result, but indicates the algorithm is a perfect forecast for the occurrence of a non-event. FAR is used to determine the accuracy of the forecasting algorithm. Critical skill index,

CSI, is an evaluation of the skill of a forecast algorithm as determined by the ratio of correctly forecasted events to the total number of observed events. One is an ideal score that indicates a perfect forecasting algorithm. The Operational Utility Index (OUI) is a nonstandard performance metric developed by the 45th Weather Squadron at Kennedy Space Center, FL (DeArcangelo 2000). This skill score is calculated by $OUI = [(3 * POD) + (2 * TSS) + (-1 * FAR)] / 6$. TSS is the true skill score, another skill score examining the accuracy of a forecasting algorithm. A perfect OUI score is 0.83, with a failing score of 0 or less. The different skill scores used in OUI are weighted according to their significance to operations at KSC. The weights applied to POD, TSS, and FAR were set subjectively by operators at 45 WS. POD gets the highest weight since lightning prediction is so important to personnel safety to 45 WS customers. TSS gets a moderate weight since skill is also important to the economic interests of 45 WS customers. Finally, FAR gets the least weight since reducing false alarms is the least important goal given the importance of personnel safety to 45 WS.

Table 3 suggests, as expected, that the more stringent the requirement is made for a threshold to be met, the smaller the lead time and the lower POD. This is particularly evident in decreasing lead times and POD associated with applying decreasing temperature (increasing height) thresholds. The reflectivity threshold of 35 dBZ at -10°C has the best lead time with high POD. However, this algorithm is also associated with the greatest FAR. 40 dBZ at -15°C is the best reflectivity based forecasting algorithm determined by the perfect POD, FAR, and OUI. It does not result in a large lead time, thus if a forecaster is more interested in a strong lead time, 35 dBZ at -10°C might be found a more ideal algorithm in such a situation. The lead times of Z_h and temperature are comparable to previous studies. Secondary reflectivity levels reduce FAR while maintaining lead-time and POD compared to the benchmark.

The best Z_{DR} column algorithm is $Z_{DR} > 1$ dB and 40 dBZ at -10°C . Compared to the benchmark, FAR is reduced by about half, increasing CSI and OUI with an increase in lead time by approximately 0.5 minutes. This supports the utility of dual-polarimetric variables in first flash forecasting. The difference between 40 dBZ reflectivity at -10°C and the best Z_{DR} column algorithm is found in the reduction of POD and lead time difference stems from two

missed Z_{DR} column forecasts. On the other hand, the leading Z_{DR} column algorithm results in a lead time that is greater than the best reflectivity forecasting method. If a forecaster is more concerned with an increased lead time at the expense of decreased skill, Z_{DR} column algorithm forecasting is a useful approach. This increase of half a minute, however, is only a marginal increase and is not significant to general forecasting advancement.

When examining PID categories and time evolution of the cells in these cases, ice and snow are dominant initially, followed by the formation of graupel, which is also observable in the Z_{DR} value trends in Fig. 5. PID categories containing hail in smaller quantities are present just prior to first flash. The first instance of graupel PID and supercooled drops PID is found to have similar results. In general, the trigger for the first instance of graupel is a graupel and rain mixture PID as is for the detection of supercooled drops PID. This leads to similar results between the two algorithms. However, even in presence of these similarities, the best algorithm of the PID forecasting category based on skill scores and lead time is the detection of the first instance of graupel PID at -15°C . However weighting lead time over skill, the better forecasting algorithm of this group is the detection of graupel PID at -10°C . The lead time of graupel and supercooled drops PID at -10°C results in about a minute increase in average lead time. Comparison of lead time and skill scores of PID and the benchmark (40 dBZ at -10°C) shows a reduction of FAR and increased CSI, which supports the conclusion that dual-polarimetric variables are useful in first flash forecasting though without a significant improvement to current forecasting algorithms.

This study shows a marginal increase in skill resulting from a decrease in FAR using dual-polarimetric variables such as Z_{DR} column and PID signatures in comparison to a benchmark of 40 dBZ at -10°C representing typical radar reflectivity forecasting algorithms. In general, the decrease of FAR is also associated with a decrease in POD. Though the accuracy of correctly determining a non-occurring event is increased, there is also a resulted decrease in POD. In general, for safety, it is more advantageous to positively identify a weather event, than to accurately identify a non-event. The limited data set also concludes a marginal increase in lead time associated with dual-polarimetric variable forecasting. The lead time gained by the use of dual-polarimetric variables

is in general approximately half a minute. This does not provide a significant increase. An increase of five minutes would significantly improve forecast warnings, however half a minute provides little improvement. The utility of the PID algorithm is found in the flexibility of hydrometeor identification by the fuzzy-logic approach compared to the hard set thresholds of such algorithms as the Z_{DR} column. The best method for detection based on high POD and reduced FAR is 40 dBZ at -15°C . However, the best method for detection based on a strong lead time and skill, (e.g., CSI) is graupel PID at -15°C . Depending on the need of the user, dual-polarimetric variables can be more advantageous than basic radar reflectivity based forecasting algorithms.

Errors in results may derive from the subjective methodology of selecting area of interest. Potential bias also originates from the limited sample size. Furthermore, some bias maybe inherent in the PID algorithm optimization. For these reasons further work should be conducted.

4. FUTURE WORK

To further determine the utility of dual-polarimetric variables this study should be expanded. A data set including different meteorological and convective situations such as multicellular structures could provide further support and reduce sample biases. To do so, cell selection should be automated to reduce possible sample biases and enabling analysis of a larger data set. Another possibility for future work is to compare dual-polarization techniques against other aspects of the 45 WS approach, including depth and duration of reflectivity thresholds relative to temperature levels. To further develop the utility of dual-polarimetric variables, this study should be replicated in different geographical regions. To determine the cost-benefit of dual-polarimetric variables a similar study should be conducted in real-time operations. Finally, the PID algorithm should be optimized and tuned for accuracy to determine the true value of this tool.

5. ACKNOWLEDGMENTS

We would like to acknowledge the assistance of Chris and Elise Schultz, Mariana Felix, Matthew Anderson and Patrick Gatlin for

assistance with ARMOR radar scanning and data analysis. Support provided by National Oceanic and Atmospheric Administration (NOAA) Collaborative Science, Technology, and Applied Research Program (CSTAR), and National Aeronautics and Space Administration (NASA) Marshal Spaceflight Center (MSFC).

6. REFERENCES

- Bringi, V. N., K. Knupp, A. Detwiler, L. Liu, I. J. Caylor, R. A. Black, 1997: Evolution of a Florida Thunderstorm during the Convection and Precipitation/Electrification Experiment: The Case of 9 August 1991. *Mon. Wea. Rev.*, **125**, 2131–2160.
- Bringi, V. N., T. D. Keenan, and V. Chandrasekar, 2001: Correcting C-band radar reflectivity and differential reflectivity data for rain attenuation: A self-consistent method with constraints. *IEEE Trans. Geosci. Remote Sens.*, **39**, 1906–1915.
- Bringi, V. N., and V. Chandrasekar, 2001: *Polarimetric Doppler Weather Radar: Principles and Applications*. Cambridge University Press.
- Buechler, D. E., and S. J. Goodman, 1990: Echo size and asymmetry: Impact on NEXRAD storm identification. *J. Appl. Meteor.*, **29**, 962–969.
- Carey, L. C., and S. A. Rutledge, 1996: A multiparameter radar case study of the microphysical and kinematic evolution of a lightning producing storm. *Meteor. Atmos. Phys.*, **59**, 33–64.
- Carey, Lawrence D., and Steven A. Rutledge, 2000: The Relationship between Precipitation and Lightning in Tropical Island Convection: A C-Band Polarimetric Radar Study. *Mon. Wea. Rev.*, **128**, 2687–2710.
- Church, C.R., 1966: The electrification of hail. Ph.D. thesis. Universtiy of Durham, 55-57.
- D’Arcangelo, D. L., 2000: Forecasting The Onset Of Cloud-Ground Lightning Using Layered Vertically Integrated Liquid Water. M. S. Thesis, Pennsylvania State University, Aug 00, 60 pp.
- Deierling, W., W. A. Petersen, J. Latham, S. Ellis, and H. J. Christian, 2008: The relationship between lightning activity and ice fluxes in thunderstorms. *J. Geophys. Res.*, **113** (D15), D15210, doi:10.1029/2007JD009700.

- Dye, J.E., J.J. Jones, A.J. Weinheimer, W.P. Winn, 1992: Reply to comments by C. B. Moore and B. Vonnegut: further analysis of two regions of charge during initial thunderstorm electrification. *Quart. J. Roy. Meteor. Soc.*, **118**.
- Dye, J. E., J.-J. Jones, A. J. Weinheimer, and W. P. Winn, 1988: Observations within two regions of charge during initial thunderstorm electrification. *Quart. J. Roy. Meteor. Soc.*, **114**, 1271–1290.
- Dye, J. E., J.J. Jones, W. P. Winn, T. A. Cerni, B. Gardiner, D. Lamb, R. L. Pitter, J. Hallett, and C. P. R. Saunders, 1986: Early electrification and precipitation development in a small, isolated Montana cumulonimbus. *J. Geophys. Res.*, **91**, 1231-1247.
- Dye, J. E., W. P. Winn, J. J. Jones, and D. W. Breed, 1989: The electrification of New Mexico thunderstorms. Part 1: Relationship between precipitation development and the onset of electrification. *J. Geophys. Res.*, **94**, 8643–8656.
- Goodman, S. J., D. E. Buechler, P. D. Wright, and W. D. Rust, 1988: Lightning and precipitation history of a microburst-producing storm, *Geophys. Res. Lett.*, **15**, 1185-1188.
- Goodman, S. J., and Coauthors, 2005: The North Alabama Lightning Mapping Array: Recent severe storm observations and future prospects. *Atmos. Res.*, **76**, 423-437.
- Gremillion M. S., and R. E. Orville, 1999: Thunderstorm characteristics of cloud-to-ground lightning at the Kennedy Space Center, Florida: A study of lightning initiation signatures as indicated by WSR-88D. *Wea. Forecasting*, **14**, 640–649.
- Jameson, A. R., M. J. Murphy, and E. P. Krider, 1996: Multiple-parameter radar observations of isolated Florida thunderstorms during the onset of electrification. *J. Appl. Meteor.*, **35**, 343–354.
- Jolliffe, I. T., and D. B. Stephenson, 2003: *Forecast Verification: A Practitioner's Guide in Atmospheric Science*. John Wiley and Sons.
- Keith, W. D. and C. P. R. Saunders, 1990: Further laboratory studies of the charging of graupel during ice crystal interactions. *Atmos. Res.*, **25**, 445–464.
- Larsen, H. R., and E. J. Stansbury, 1974: Association of lightning flashes with precipitation cores extending to height 7 km. *J. Atmos. Terr. Phys.*, **36**, 1547–1553.
- Lhermitte, R., and P. R. Krehbiel, 1979: Doppler radar and radio observations of thunderstorms. *IEEE Trans. Geosci. Electron.*, **GE-17**, 162-171.
- Lim, S., V. Chandrasekar, and V. N. Bringi, 2005: Hydrometeor classification system using dual-polarization radar measurements: Model improvements and in situ verification. *IEEE Trans. Geosci. Remote Sens.*, **43**, 792–801.
- Lund, N. R., D. R. MacGorman, T. J. Schuur, M. I. Biggerstaff, and W. D. Rust, 2009: Relationships between lightning location and polarimetric radar signatures in a small mesoscale convective system. *Mon. Wea. Rev.*, **137**, 4151–4170.
- MacGorman, D.R., and W.D. Rust, 1998: *The Electrical Nature of Storms*. Oxford University Press.
- McCaul, E. W., Jr., J. Bailey, J. Hall, S. J. Goodman, R. J. Blakeslee, and D. E. Buechler, 2005: A flash clustering algorithm for North Alabama Lightning Mapping Array data. *Preprints, Conf. on Meteorological Applications of Lightning data*, San Diego, CA, Amer. Meteor. Soc., 5.2.
- McNamara, T. M., W. P. Roeder, and F. J. Merceret, 2010: The 2009 update to the lightning launch commit criteria, 14th Conference on Aviation, Range, and Aerospace Meteorology, 17-21 Jan 10, Paper 469, 16 pp.
- National Weather Service, cited 2010: Natural Hazard Statistics. [<http://www.nws.noaa.gov/om/hazstats.shtm>]
- Petersen, W. A., S. A. Rutledge, and R. E. Orville. 1996: Cloud-to-ground lightning observations from TOGA COARE: Selected results and lightning location algorithms. *Mon. Wea. Rev.* **124**:602–620.
- Petersen, W. A., K. R. Knupp, D. J. Cecil, and J. R. Mecikalsi, 2007: The University of Alabama Huntsville THOR Center instrumentation: Research and operational collaboration. *33rd International Conference on Radar Meteorology*, American Meteorological Society, Cairns, Australia, August 6-10, 2007.

- Reynolds, S. E., Brook, M. and Gourley, M. F., 1957: Thunderstorm charge separation. *J. Met*, **14**, 426–436.
- Roeder, W. P., and C. S. Pinder, 1998: Lightning forecasting empirical techniques for central Florida in support of America's space program. *16th Conference On Weather Analysis And Forecasting*, 11-16 Jan 98, 475-477
- Rutledge, Steven A., Walter A. Petersen, 1994: Vertical Radar Reflectivity Structure and Cloud-to-Ground Lightning in the Stratiform Region of MCSs: Further Evidence for In Situ Charging in the Stratiform Region. *Mon. Wea. Rev.*, **122**, 1760–1776.
- Ryzhkov, A. V., S. E. Giangrande, V. M. Melnikov, and T. J. Schuur, 2005: Calibration issues of dual-polarization radar measurements. *J. Atmos. Ocean. Tech.*, **22**, 1138-1155.
- Saunders, C. P. R., W. D. Keith, and R. P. Mitzeva, 1991: The effect of liquid water on thunderstorm charging. *J. Geophys. Res*, **96**, 11007–11017.
- Takahashi, T., 1978: Riming electrification as a charge generation mechanism in thunderstorms. *J. Atmos. Sci*, **35**, 1536–1548.
- Vincent, B.R, L.D. Carey, D. Schneider, K. Keeter and R. Gonski, 2003: Using WSR-88D reflectivity data for the prediction of cloud-to-ground lightning: A North Carolina study. *Nat. Wea. Digest*, **27**, 35-44.
- Vivekanandan, J., D. S. Zrnic, S. M. Ellis, R. Oye, A. V. Ryzhkov, and J. Straka, 1999: Cloud microphysics retrieval using S-band dual-polarization radar measurements. *Bull. Amer. Meteor. Soc.*, **80**, 381–388.
- Weems, J. W., C. S. Pinder, W. P. Roeder, and B. F. Boyd, 2001: Lightning watch and warning support to spacelift operations. *18th Conference on Weather Analysis and Forecasting*, 30 Jul – 2 Aug 01, 301-305.
- Wolf, P., 2007: Anticipating the Initiation, cessation, and frequency of cloud-to-ground lightning, utilizing WSR-88D Reflectivity Data. *Electronic Journal of Operational Meteorology*.
- Workman, E. J., and S. E. Reynolds, 1949: Electrical activity as related to thunderstorm cell growth. *Bull. Amer. Meteor. Soc.*, **30**, 142–144.
- Yang, Y.H., P. King, 2010: Investigating the Potential of Using Radar Echo Reflectivity to Nowcast Cloud-to-Ground Lightning Initiation over Southern Ontario. *Weather and Forecasting*, **25**:4, 1235-1248.

Table 1. Table of lightning initiation algorithms tested on the radar data set. The test focus column indicates the variables used for the test. The thresholds column contains the various parameters used to compose the algorithms. Each parameter is then paired with each thermal threshold level found in the third column. The final column describes the observation requirements.

Focus	Thresholds	Thermal levels	
Zh and temperature	35, 40, 45 dBZ	-10, -15, -20 °C	First occurrence of Highest value
2nd level Zh and temperature (1st level Zh > 30 dBZ)	15, 20, 25 dBZ	8 km	First occurrence of Highest value
Z _{DR} and Z _h with temperature (Zh >40 dBZ)	>1dB	-10, -15, -20 °C	First instance of Highest value
PID and temperature	PID = 8,9 (graupel) PID = 7,9,14 (supercool drops)	-10, -15, -20 °C	First instance of PID value

Table 2. 17 bulk hydrometeor categories of the modified NCAR PID algorithm categories.


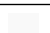

Category	Color	NCAR PID
1		Cloud
2		Drizzle
3		Light Rain
4		Moderate Rain
5		Heavy Rain
6		Hail
7		Rain and Hail
8		Graupel and Small Hail
9		Graupel and Rain
10		Dry Snow
11		Wet Snow
12		Ice Crystals
13		Irregular Ice Crystals
14		Supercooled Liquid
15		Flying Insects
16		Second Trip
17		Ground Clutter

Table 3. Results of the reflectivity threshold algorithms. Skill scores include, probability of detection (POD), false alarm ratio (FAR), operational utility index (OUI), critical success index (CSI), and average lead time. The first column indicates the forecasting algorithm associated with each score set.

	POD	FAR	OUI	CSI	Lead Time
35 dbz at -10°C	1	0.2439	0.6172	0.7561	12.5
40 dbz at -10°C	1	0.2051	0.6588	0.7949	10.5
45 dbz at -10°C	0.9677	0.0909	0.7387	0.8824	10
35 dbz at -15°C	1	0.0606	0.7881	0.9394	9.5
40 dbz at -15°C	1	0	0.8333	1	8
45 dbz at -15°C	0.9032	0	0.7527	0.9032	5
35 dbz at -20°C	0.9677	0.0323	0.7835	0.9375	5
40 dbz at -20°C	0.9032	0	0.7527	0.9032	4
45 dbz at -20°C	0.5161	0	0.4301	0.5161	2
15 dBZ above 8 km	0.9677	0.1176	0.7167	0.8571	10.5
20dBZ above 8 km	0.9677	0.0909	0.7387	0.8824	9
25dBZ above 8 km	0.9677	0.0625	0.7609	0.9091	7.5

Table 4. Results of the Z_{DR} column algorithms. Skill scores include, probability of detection (POD), false alarm ratio (FAR), operational utility index (OUI), critical success index (CSI), and average lead time. The first column indicates the forecasting algorithm associated with each score set.

	POD	FAR	OUI	CSI	Lead Time
40 dBZ at -10°C	1	0.2051	0.6588	0.7949	10.5
$Z_{dr} > 1$ dB at -10°C	0.9355	0.0938	0.7113	0.8529	11
$Z_{dr} > 1$ dB at -15°C	0.8065	0	0.672	0.8065	6.5
$Z_{dr} > 1$ dB at -20°C	0.3226	0	0.2688	0.3226	2

Table 5. Results of the PID test algorithms. Skill scores include, probability of detection (POD), false alarm ratio (FAR), operational utility index (OUI), critical success index (CSI), and average lead time. The first column indicates the forecasting algorithm associated with each score set.

	POD	FAR	OUI	CSI	Lead Time
40 dBZ at -10°C	1	0.2051	0.6588	0.7949	10.5
Graupel					
8,9 at -10°C	1	0.1842	0.6798	0.8158	11.5
8,9 at -15°C	0.9355	0.0333	0.7565	0.9063	9.5
8,9 at -20°C	0.9032	0.0345	0.7294	0.875	4
Supercooled Drops					
7,9,14 at -10°C	0.9677	0.1429	0.6949	0.8333	11.5
7,9,14 at -15°C	0.871	0.0357	0.7023	0.8438	7
7,9,14 at -20°C	0.7097	0	0.5914	0.7097	3

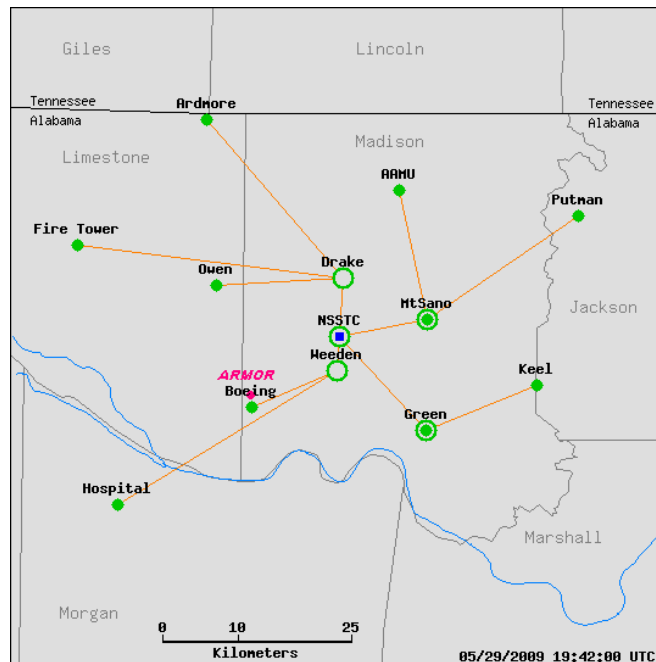


Figure 1. Map of the North Alabama Lightning Mapping Array, the NALMA consists of 10 TOA VHF sensors centered on the NSSTC. Locations of the sensors are indicated by green dots, green circles indicate locations of relay centers, the base station is indicated with the blue square, and the pink dot indicates the location of ARMOR relative to the array.

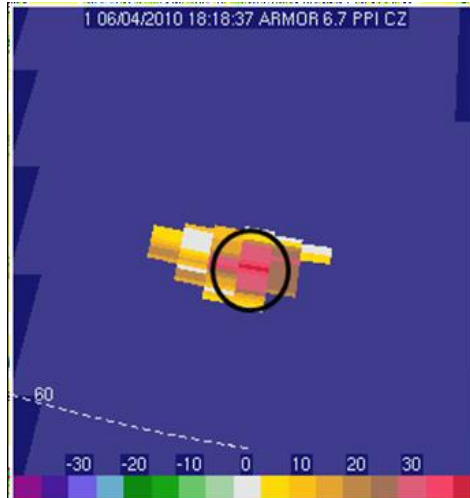


Figure 2. Larsen area of cell 1 of case 20100604 is indicated by the black circle. The Larsen area is defined as the reflectivity threshold ($\geq 30\text{dBZ}$) at thermal threshold (-10°C) estimated by the reflectivity echo and radius required to encompass the majority of the threshold reflectivity gates. The temperature level of the radar scan is at approximately -10°C .

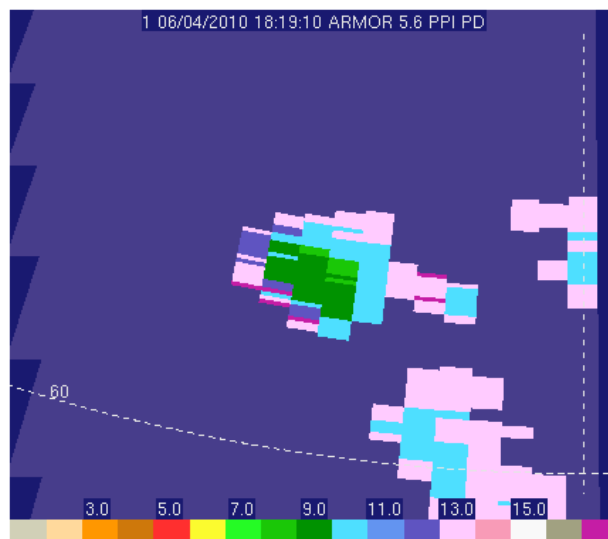


Figure 3. First instance of graupel PID signature in cell 1 of case 20100604 at approximately -10°C .

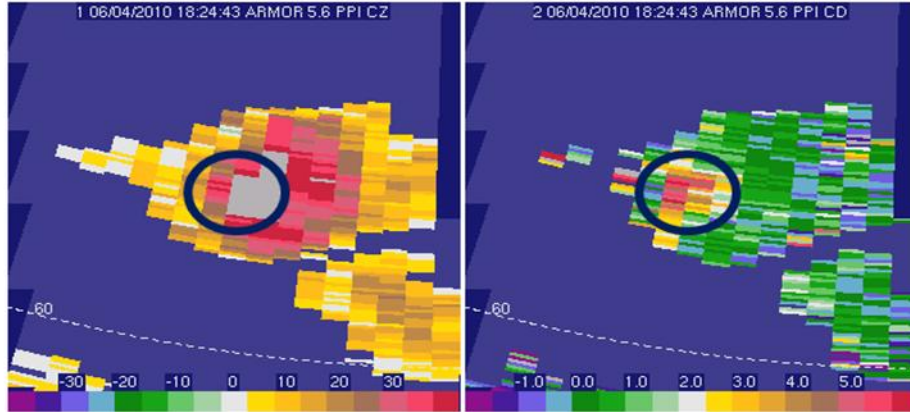
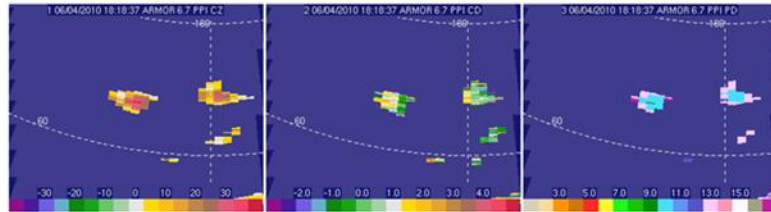
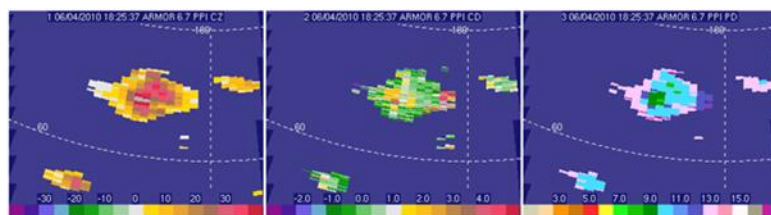


Figure 4. An example of a Z_{DR} column indicated by the black circles. The enhanced values of Z_{DR} , ≥ 1 dB, associated with high values of Z_h , ≥ 40 dBZ, indicate oblique liquid particles at temperatures below freezing. The altitude of the radar scan is approximately 5.64 km at an environmental temperature of approximately -8.5°C .

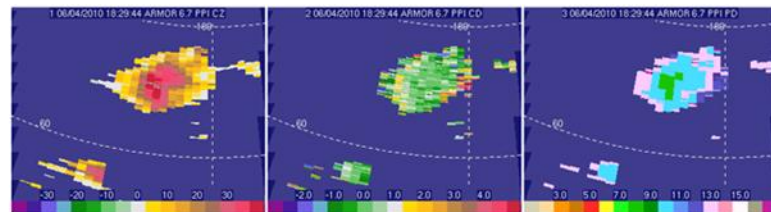
a) Initial development and first Lasren area signature



b) Formation of significant precipitation, note graupel and rain indicated in the PID, and the enhanced values of Z_{dr} associated with enhanced Z_h values



c) The freezing of the Z_{dr} column seen in the decreased Z_{dr} values, PID indicates the presence of graupel and small hail.



d) A CG flash occurs before the first IC strike at approximately 1837UTC

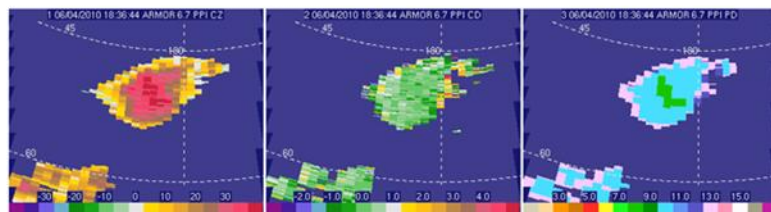


Figure 5. Evolution of cellular and precipitation development as seen by Z_h , Z_{DR} and PID (left to right) in the thunderstorm cell 1 of case 20100604 at approximately -10°C thermal level. UTC times of each figure: a) 181837, b)182537, c) 182944, and d) 183644.